AGU PUBLICATIONS

Water Resources Research

RESEARCH ARTICLE
10.1002/2016WR019850

Key Points:
- Oxygenation increases sediment oxygen flux due to elevated oxygen concentrations at the SWI and thinning of the DBL
- In situ measurements are compared to predictive models of sediment oxygen flux
- Three interfacial flux models agree with in situ sediment oxygen flux measurements

Supporting Information:
- Supporting Information S1

Correspondence to:
J. C. Little,
jcl@vt.edu

Citation:
Bierlein, K. A., M. Rezvani, S. A. Socolofsky, L. D. Bryant, A. Wüest, and J. C. Little (2017), Increased sediment oxygen flux in lakes and reservoirs: The impact of hypolimnetic oxygenation, *Water Resour. Res.*, *53*, 4876–4890, doi:10.1002/2016WR019850.

Received 27 SEP 2016
Accepted 19 MAY 2017
Accepted article online 24 MAY 2017
Published online 15 JUN 2017

Increased sediment oxygen flux in lakes and reservoirs: The impact of hypolimnetic oxygenation

Kevin A. Bierlein[1,2], Maryam Rezvani[3], Scott A. Socolofsky[3], Lee D. Bryant[4], Alfred Wüest[5,6], and John C. Little[1]

[1]Department of Civil and Environmental Engineering, Virginia Tech, Blacksburg, Virginia, USA, [2]Hydros Consulting, Boulder, Colorado, USA, [3]Zachry Department of Civil Engineering, Texas A&M University, College Station, Texas, USA, [4]Department of Architecture and Civil Engineering, University of Bath, Bath, UK, [5]Eawag, Swiss Federal Institute of Aquatic Science and Technology, Kastanienbaum, Switzerland, [6]Physics of Aquatic Systems Laboratory, Swiss Federal Institute of Technology (EPFL), ENAC-APHYS, Lausanne, Switzerland

Abstract Hypolimnetic oxygenation is an increasingly common lake management strategy for mitigating hypoxia/anoxia and associated deleterious effects on water quality. A common effect of oxygenation is increased oxygen consumption in the hypolimnion and predicting the magnitude of this increase is the crux of effective oxygenation system design. Simultaneous measurements of sediment oxygen flux (J_{O2}) and turbulence in the bottom boundary layer of two oxygenated lakes were used to investigate the impact of oxygenation on J_{O2}. Oxygenation increased J_{O2} in both lakes by increasing the bulk oxygen concentration, which in turn steepens the diffusive gradient across the diffusive boundary layer. At high flow rates, the diffusive boundary layer thickness decreased as well. A transect along one of the lakes showed J_{O2} to be spatially quite variable, with near-field and far-field J_{O2} differing by a factor of 4. Using these in situ measurements, physical models of interfacial flux were compared to microprofile-derived J_{O2} to determine which models adequately predict J_{O2} in oxygenated lakes. Models based on friction velocity, turbulence dissipation rate, and the integral scale of turbulence agreed with microprofile-derived J_{O2} in both lakes. These models could potentially be used to predict oxygenation-induced oxygen flux and improve oxygenation system design methods for a broad range of reservoir systems.

1. Introduction

Seasonal oxygen depletion is a common and significant water-quality issue affecting many thermally stratified lakes. Dissolved oxygen (DO) is depleted in the water column and the lake sediment by many processes, including oxidation of both organic detritus and reduced chemical species. Low DO in the hypolimnion can lead to the release of phosphorus, nitrogen, methyl-mercury, hydrogen sulfide, iron, and manganese from the sediments due to a number of anaerobic biogeochemical mechanisms [*Funkey et al.*, 2014; *Testa and Kemp*, 2012; *Gantzer et al.*, 2009a; *Beutel et al.*, 2008; *Davison*, 1993]. Increased phosphorus and nitrogen concentrations can stimulate algal growth, which then lead to additional oxygen demand due to mineralization of dead algal biomass. Methylmercury is extremely toxic to aquatic life and capable of bioaccumulating in higher trophic levels. Hydrogen sulfide, iron, and manganese increase oxidant costs during drinking water treatment and can cause problems associated with taste, odor, and color if not adequately removed during treatment [*American Water Works Association*, 2010; *Kohl and Medlar*, 2003].

Sediment oxygen uptake (J_{O2}) is a primary sink for DO in the hypolimnion [*Schwefel et al.*, 2016; *Müller et al.*, 2012]. This flux is partly controlled by the presence of a diffusive boundary layer (DBL) immediately above the sediment, which restricts the transport of DO from the bulk hypolimnion into the sediment. J_{O2} is also a function of the DO gradient between the bulk hypolimnetic water and the DO concentration at the sediment-water interface (SWI); an increased concentration gradient drives increased diffusive transport across the DBL and into the sediment.

Several studies have confirmed the importance of the DBL in controlling J_{O2}. Laboratory experiments using sediment core incubations linked changes in DBL thickness (δ_{DBL}) and J_{O2} to water velocity [*Moore et al.*, 1996; *Beutel*, 2003]. Recent field studies showed J_{O2} responding to changes in near-sediment turbulence as

a result of natural seiche activity [*Lorke et al*., 2003; *Bryant et al*., 2010a], with the turbulence dissipation rate found to be the primary driver to DBL changes rather than current velocity. As observed by *Bryant et al*. [2010a], when turbulence increases, the DBL above the sediment becomes thinner, thereby decreasing resistance to diffusive transport of DO across the SWI and increasing J_{O2}. Conversely, during relatively quiescent periods the DBL thickens, resulting in decreased J_{O2}. Using in situ oxygen microprofiles, *Bryant et al*. [2010a] observed changes in J_{O2} on an hourly timescale by a factor of approximately 6 in response to changes in near-sediment turbulence and δ_{DBL}.

Hypolimnetic oxygenation, an aeration/oxygenation strategy designed to preserve thermal stratification, is increasingly used to replenish hypolimnetic DO. Various systems are used, including Speece Cones, airlift aerators, side-stream supersaturation systems, and bubble-plume diffusers, to introduce DO into the hypolimnion [*Beutel and Horne*, 1999; *Singleton and Little*, 2006]. Bubble plumes, one of the more common types, are generally linear or circular and can be designed to inject either air (aeration) or oxygen gas (oxygenation) into the hypolimnion at a relatively low gas flow rate. In deeper lakes, when using oxygen gas, most of the bubbles dissolve within the hypolimnion and the upward momentum generated by the plume is low enough to prevent significant disruption of the thermocline. When correctly designed and operated, these systems are often very successful at mitigating hypoxia and its associated effects [*Beutel*, 2006; *Gantzer et al*., 2009a; *Liboriussen et al*., 2009; *Debroux et al*., 2012; *Müller et al*., 2014]. In addition to increased hypolimnetic DO concentrations, bubble-plume operation can also result in enhanced turbulent mixing on localized scales in lakes and reservoirs. This additional turbulence could locally drive decreases in δ_{DBL}, and thus increase J_{O2}, in a manner similar to that observed in naturally forced lakes such as Lake Alpnach [*Lorke et al*., 2003; *Bryant et al*., 2010a].

A common effect of bubble-plume oxygenation is increased oxygen consumption, both within the hypolimnetic water and the sediment. Increased DO uptake has been attributed to enhanced DO availability facilitating elevated rates of organic matter mineralization. Work by *Gantzer et al*. [2009b], which investigated oxygen depletion rates in two water-supply reservoirs, showed that hypolimnetic oxygen demand (HOD) increases as a function of the gas flow rate applied to the oxygen diffusers. In larger lakes and reservoirs where the oxygenation system flow rate is small relative to the hypolimnion DO content, the total hypolimnetic oxygen demand may not respond as strongly to increases in gas flow rate [*Gantzer et al*., 2009b]. HOD is intrinsically linked to oxygen uptake by the sediment, i.e., J_{O2}, particularly in lakes with a high ratio of sediment area to hypolimnion volume. The rate of labile carbon oxidation in the sediment dictates the sediment's DO requirements up to the point at which oxygen transport into the sediment becomes limiting. As such, the rate of labile carbon oxidation can have significant influence on DO dynamics and uptake (i.e., depletion) within the hypolimnion [*Higashino et al*., 2004]. Oxygen-induced increases in J_{O2} are linked to (1) elevated hypolimnetic DO concentrations and (2) decreased δ_{DBL} which result in an increased DO gradient across the DBL and correspondingly enhanced rates of diffusive transport through the DBL. It is critical that these increases in DO uptake are taken into account when designing and implementing oxygenation management strategies.

While effective at adding DO, bubble plumes also add energy to the hypolimnion via enhancing mixing in the near field and generating large-scale circulation patterns, as observed in field experiments and computer simulations. *McGinnis et al*. [2004] used both field data and computer simulation results to highlight enhanced mixing in the bubble-plume near field as a result of diffuser operation. Computer simulations by *Singleton et al*. [2010] demonstrated the ability of bubble-plume oxygenation systems to drive circulation of hypolimnetic water throughout the hypolimnion in a small water-supply reservoir, even at low gas flow rates. Field observations by *Bryant et al*. [2011a] demonstrated the importance of these large-scale currents in supplying oxygenated water to the SWI in the far field. J_{O2} was observed to rapidly decrease at a study site $\sim$0.7 km from a bubble-plume diffuser after turning the system off, yet required approximately 5 days for currents to reestablish and replenish the SWI with oxygenated water once the diffuser was turned back on. As bubble plumes have been found to affect hypolimnetic mixing and DO concentrations in the near and far fields, their influence on J_{O2} is very likely to be spatially variable as well (as shown by *Bryant et al*. [2011a]).

Despite the current level of understanding of how bubble plumes impact lake hydrodynamics and DO distribution, it remains difficult to accurately predict bubble-plume-induced J_{O2} when designing a bubble-plume oxygen diffuser. Current best practice is to use an induced J_{O2} multiplier as a "factor of safety,"

typically between 2 and 4, as suggested by *Moore et al*. [1996], *Beutel* [2003], and others. This approach is not ideal, given that it is based on empirical equations derived from laboratory experiments, rather than being based on in situ data or mechanistic models. As hypolimnetic oxygenation becomes more widely used, there is a need to improve the ability to estimate induced J_{O2} and HOD.

This study aims to investigate the effect of diffuser flow rate on both δ_{DBL} and J_{O2} near the diffuser, as well as the spatial and temporal variability of J_{O2}. Furthermore, it compares in situ measurements of J_{O2} to physical models of interfacial flux evaluated using in situ velocity and turbulence measurements to determine which of the models, if any, may be appropriate for predicting J_{O2} in oxygenated lakes. An appropriate model of J_{O2} could improve our ability to predict DO dynamics and depletion rates within aerated lakes and reservoirs, thereby improving and optimizing oxygenation system design, operation, and management.

2. Methods

2.1. Study Sites

2.1.1. Carvins Cove Reservoir

Carvins Cove Reservoir (CCR) is a eutrophic water-supply reservoir in southwestern Virginia, USA, which serves as one of the primary sources of drinking water for the City of Roanoke (Table 1). A hypolimnetic oxygenation system consisting of two linear bubble-plume diffusers, which bubble oxygen gas into the hypolimnion, was installed near the water-treatment plant intake in 2005 to mitigate episodic increases in iron and manganese stemming from seasonal hypoxia. The oxygenation system has been quite successful at maintaining adequate hypolimnetic DO and preventing hypoxic release of reduced iron and manganese [*Gantzer et al*., 2009a, 2009b; *Bryant et al*., 2011a, 2011b].

From 26 May to 2 June 2013, a microprofiler (MP4; Unisense A/S) was deployed approximately 30 m from the midpoint of the oxygenation system to collect in situ microprofiles of DO in the bottom boundary layer (Figure 1a). The field campaign was designed to capture the effect of the bubble-plume diffuser flow rate on δ_{DBL} and J_{O2}. The diffuser had been operating at 30.6 $Nm^3\ h^{-1}$ for approximately 6 weeks prior to the deployment of the field equipment on 26 May. Beginning on 27 May, the flow rate was adjusted once each day. The diffuser flow rate was adjusted to 68, 51, 34, 17, 0, and 23 $Nm^3\ h^{-1}$, in sequence over the course of the 8 day campaign, covering the entire range of flow rates for which the oxygenation system was designed. Hydrodynamics and other processes in the water column respond quickly enough in the diffuser near-field, where the microprofiler was deployed, to allow for daily adjustments of the diffuser flow rate. Daily adjustments also allow sufficient time for DO concentrations in the sediment to equilibrate, since DO residence times in the sediment are much shorter. For example, *Bryant et al*. [2010a] calculated residence times of less than 10 min in the sediment of a mesoeutrophic lake (Lake Alpnach, Switzerland). An acoustic Doppler velocimeter (ADV; Vector; Nortek) was deployed on a separate mooring alongside the microprofiler and measured three-dimensional water velocity (longitudinal, transversal, and vertical) approximately 15 cm above the SWI at 16 Hz.

2.1.2. Lake Hallwil

Lake Hallwil (LH) is a medium-sized lake located on the Swiss Plateau, north of Lucerne, Switzerland (Table 1). Early in the 20th century, agricultural-driven and wastewater-driven phosphorous loading increased and led to excessive algal production and seasonal anoxia in the hypolimnion of LH [*Holzner et al*., 2012]. In 1985, six circular diffusers, each 6.5 m in diameter and arranged in a 300 m diameter circular configuration, were installed in the deep, central region of the lake to mitigate seasonal anoxia in the hypolimnion with a target DO concentration of 4 mg L^{-1} [*Müller et al*., 2014; *Holzner et al*., 2012]. During the summer months, oxygen-enriched air is released through the diffusers at low flow rates, supplying oxygen to the hypolimnion without disrupting thermal stratification. During winter, air is released through the diffusers at high flow rates to enhance circulation and stimulate DO transfer from the atmosphere into the deep water. LH has experienced significant improvements in

Table 1. Physical Characteristics of Carvins Cove Reservoir and Lake Hallwil

	Carvins Cove Reservoir	Lake Hallwil
Max. depth (m)	22	48
Surface area (km^2)	2.5	9.95
Volume (m^3)	24×10^6	285×10^6
Elevation (m amsl)	357	449

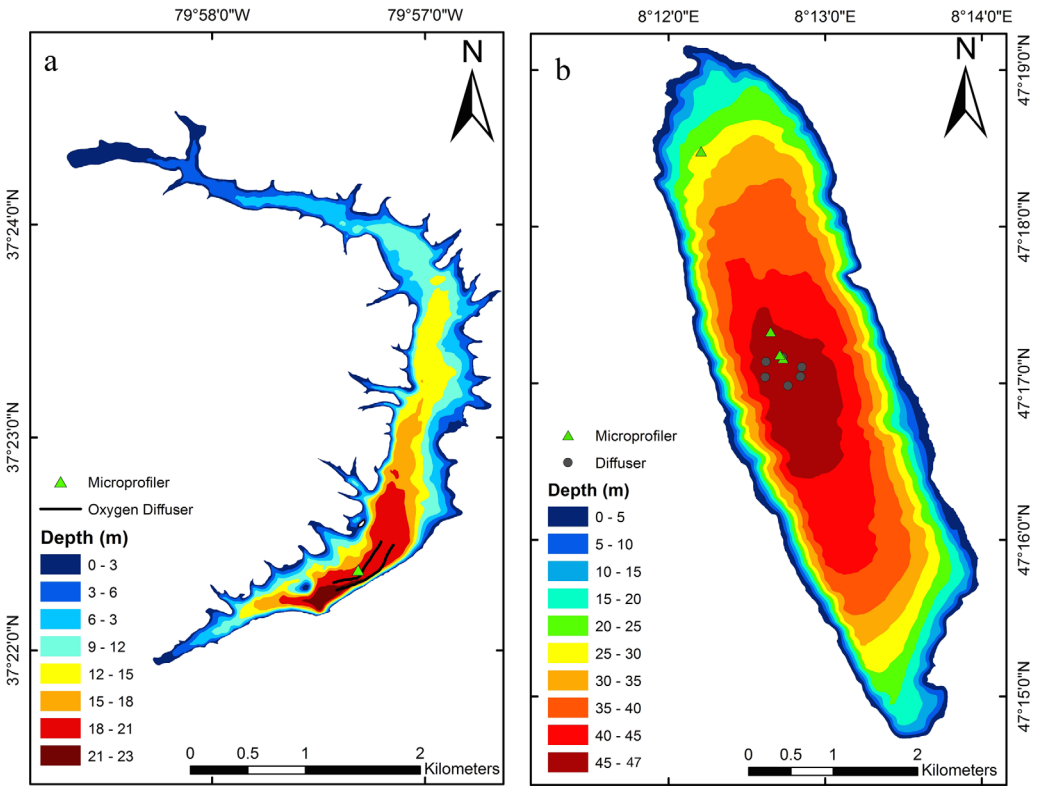

Figure 1. Bathymetric maps of (a) Carvins Cove Reservoir and (b) Lake Hallwil.

water quality since oxygenation began, though a concurrent reduction in external phosphorus loading appears to be the major driving factor in water-quality improvements [*Müller et al*., 2014].

The microprofiler was deployed at four sites in LH from 14 May to 1 June 2012 to collect in situ DO microprofiles in the DBL and investigate spatial variation in δ_{DBL} and J_{O2}. The four sites lie roughly along the main axis of the lake and are located 30, 300, and 3700 m outside the circle of diffusers, and 30 m inside the circle of diffusers (Figure 1b). While sampling at the two locations 30 m to either side of the diffuser, the oxygenation system was turned off for 2–3 days to assess the impact of diffuser operation on J_{O2} in this near-field region. During the field campaign, the diffusers were operated in summer oxygenation mode. A Nortek Vector ADV was deployed on a separate mooring alongside the microprofiler at each deployment site and measured three-dimensional water velocity approximately 15 cm above the SWI at 8 Hz.

2.2. Oxygen Flux Estimates

During both field campaigns, J_{O2} was calculated from in situ oxygen microprofiles measured with a Unisense A/S MP4 microprofiler equipped with a Clark-type DO microsensor (Unisense A/S OX-100) and a thermocouple temperature sensor (Unisense A/S TP-200). A two-point linear calibration of the temperature microsensor was performed prior to deployment using cold water brought into the field and warm water from the reservoir surface. A two-point linear calibration was also performed for the DO microsensor using zero readings from an anoxic solution (prepared using 100 mL 0.1N NaOH and 1.98 g sodium ascorbate, per Unisense recommendation) and a Winkler titration of oxygen-saturated water sampled at the reservoir surface. These calibrations were performed predeployment and postdeployment to check for sensor drift. Triplicate measurements were made at 1 Hz at the following vertical resolutions: 10 mm resolution from 100 to 10 mm above the SWI, 1 mm resolution from 10 to 5 mm above the SWI, and 0.1 mm resolution from 5 mm above the SWI to 5 mm below the SWI. The microprofiler was monitored a minimum of twice each day during deployment to adjust for settling of the instrument and to ensure the correct positioning of the microsensors with respect to the SWI. With this profiling scheme, oxygen microprofiles were obtained approximately every 50–55 min. For each profile, J_{O2} was calculated from the waterside portion using the direct method [*Bryant et al*., 2010b],

$$J_{O2} = D_w \left.\frac{\partial C}{\partial z}\right|_w = D_w \frac{C_B - C_{SWI}}{\delta_{DBL}}, \quad (1)$$

where D_w is the molecular diffusion coefficient of DO in water ($m^2\ d^{-1}$), $\partial C/\partial z|_w$ is the oxygen gradient in the DBL immediately above the SWI (mmol m^{-4}), C_B is the DO concentration in the bulk water in the bottom boundary layer (BBL) immediately above the DBL (mmol m^{-3}), and C_{SWI} is the DO concentration at the SWI (mmol m^{-3}). For the sake of comparison with J_{O2} waterside flux results based on equation (1), J_{O2} was also estimated using the sedimentside of the DO microprofile using an analogous equation [*Bryant et al*., 2010b],

$$J_{O2} = D_s \left.\frac{\partial C}{\partial z}\right|_s, \quad (2)$$

where D_s is the molecular diffusion coefficient of DO in the sediment pore water ($m^2\ d^{-1}$) and $\partial C/\partial z|_s$ is the oxygen gradient immediately (~0.1 mm) below the SWI (mmol m^{-4}). D_s is estimated as $D_s = \phi D_w$, where ϕ (m^3 voids m^{-3} volume) is the sediment porosity. Measurements of ϕ (0.96 for CCR; 0.94 for LH) were made from sediment cores collected from both lakes during previous field sampling campaigns following *Dalsgaard et al*. [2000].

The location of the SWI was determined by visually examining each profile to identify the linear region in the DBL and the change in slope associated with the difference in porosity between the water column and the sediment. Fluctuations in measurements at each point in the microprofiles were also used to aid and verify the correct positioning of the SWI, since the standard deviation in the measurements should decrease as the microsensors approach the SWI [*Bryant et al*., 2010b]. Because the exact location of the boundary between the upper DBL and the BBL can be somewhat ambiguous when analyzing oxygen microprofiles, the "effective DBL" proposed by *Jørgensen and Revsbech* [1985] was used. This approach extrapolates the oxygen gradient at the SWI until the DO concentration is equal to C_B, using this distance as δ_{DBL}.

2.3. Turbulence Estimates

Turbulence, quantified by the turbulent kinetic energy dissipation rate (ε), was calculated from the high-frequency velocity measurements collected with the ADV in the BBL using the widely accepted inertial dissipation method [*Grant et al*., 1962; *Bryant et al*., 2010a]. Dissipation rates were calculated using 50 min segments of velocity time series in both the CCR and LH campaigns, which correspond to the measurement period of the oxygen microprofiles. The velocity measurements were rotated such that the longitudinal velocity is maximized and the transversal velocities are minimized. The longitudinal velocity fluctuations were transformed to the wave number (k) domain, given as

$$E(k) = \alpha_1 \varepsilon^{2/3} k^{-5/3}, \quad (3)$$

using a value of $\alpha_1 = (18/55)$ [*Grant et al*., 1962]. This power spectrum is then multiplied by $k^{5/3}$, providing a spectrum that is dependent only on ε when $E(k) \times k^{5/3}$ is constant. The dissipation rate ε is the average of this inertial subrange.

2.4. Physical Models for Interfacial Flux

The generic form of the equation for interfacial flux is given by equation (4), where J is the flux (i.e., J_{O2} in the context of the current study), C_B is the bulk concentration, C_{SWI} is the concentration at the interface, and k_t is the transfer velocity,

$$J = k_t (C_B - C_{SWI}). \quad (4)$$

There are several available models for determining k_t. The Lewis-Whitman model [*O'Connor et al*., 2009; *Lewis and Whitman*, 1924], also known as "thin-film theory," is one of the simplest, calculating k_t as D_w/δ_{DBL}. This model is of the same form as the equations used for calculating J_{O2} from DO microprofiles (equations (1) and (2)). The film renewal model [*King*, 1966; *Danckwerts*, 1951; *Toor and Marchello*, 1958; *Higbie*, 1935] calculates k_t as

$$k_t = \sqrt{\frac{4D_w r}{\pi}}, \tag{5}$$

where r is the renewal frequency (d^{-1}), a characteristic of turbulence, and can be calculated using small-eddy or large-eddy estimates. The small-eddy estimate of r is based on the Kolmogorov timescale and can be calculated as

$$r = \sqrt{\frac{u_*^3}{hv}}, \tag{6}$$

where u_* is the shear velocity, h is the shear layer depth, and v is viscosity. The large-eddy estimate is based on the integral timescale of the turbulence (t_l) and is simply calculated as

$$r = \frac{1}{t_l}. \tag{7}$$

Many studies in the literature use a scaling relationship to estimate k_t based on the equation,

$$k_t = \alpha_2 u_* Sc^{\beta}, \tag{8}$$

where α_2 and β are empirical constants and $Sc = v/D$ is the Schmidt number. Typical values for α_2 range from 0.052 to 0.164 and values for β range often from $-7/10$ to $-2/3$, with $-2/3$ commonly used. This equation is derived from theory and scaling arguments based on the concept that k_t is a function of the dissolved species (e.g., DO) and u_*. For the current study, we use $\alpha_2 = 0.164$ and $\beta = -2/3$ to calculate k_t, following *O'Connor et al.* [2009] and *O'Connor and Hondzo* [2008a], who found these values to provide the best fit for calculating J_{O2} in a laboratory flume.

Yet another model for determining k_t was suggested by *Lorke and Peeters* [2006] and is based on the Batchelor scale [*Batchelor*, 1959]. This model calculates the transfer velocity as

$$k_t = \frac{1}{2\pi} Sc^{-1/2} (\varepsilon v)^{1/4}. \tag{9}$$

This equation has the same power-law dependence as the small eddy film renewal model. *Lorke and Peeters* [2006] proposed this model as a potential universal scaling relationship for interfacial flux. Law-of-the-wall (LOW) scaling is often assumed to be valid in the bottom boundary layer in lakes. This assumption may not always be valid, however, as wind-driven lakes may have an oscillatory boundary layer under which law-of-the-wall conditions fail to reliably predict bottom boundary layer dynamics [*Lorke and Peeters*, 2006; *Lorke et al.*, 2002]. Since this model is based on the turbulence dissipation rate, rather than friction velocity, it allows for estimates of k_t under conditions where the law-of-the-wall is not necessarily a valid assumption.

Using turbulence estimates calculated from the ADV data, the film renewal model (equation (5); using the large eddy estimate of r), the u_* scaling relationship (equation (8); hereafter referred to as the u_* model) and the *Lorke and Peeters* [2006] model (equation (9)) were used to calculate the average transfer velocity for every 24 h period of field data. This transfer velocity was then multiplied by the average difference between the bulk water DO concentration and the DO concentration at the SWI ($C_B - C_{SWI}$) as measured with the microprofiler over the same 24 h period to obtain daily estimates of J_{O2} based on these interfacial flux models. The predicted J_{O2} from these models are compared to J_{O2} calculated from the waterside of the oxygen microprofiles for each 24 h period using the root mean square error (RMSE; equation (10)),

$$RMSE = \sqrt{\frac{1}{n}\sum_{i=1}^{n} \left(J_{O2,sim_i} - J_{O2_i}\right)^2}. \tag{10}$$

3. Results and Discussion

3.1. Carvins Cove Reservoir

Twelve example DO microprofiles from the CCR deployment are shown in Figure 2. These example microprofiles show the unsteady behavior of the DO microprofiles, DO concentration overlaying the SWI (ranging from ~3 to 5 mg L^{-1}), and the DO penetration depth into the sediment (ranging from ~2 to 4 mm) over a

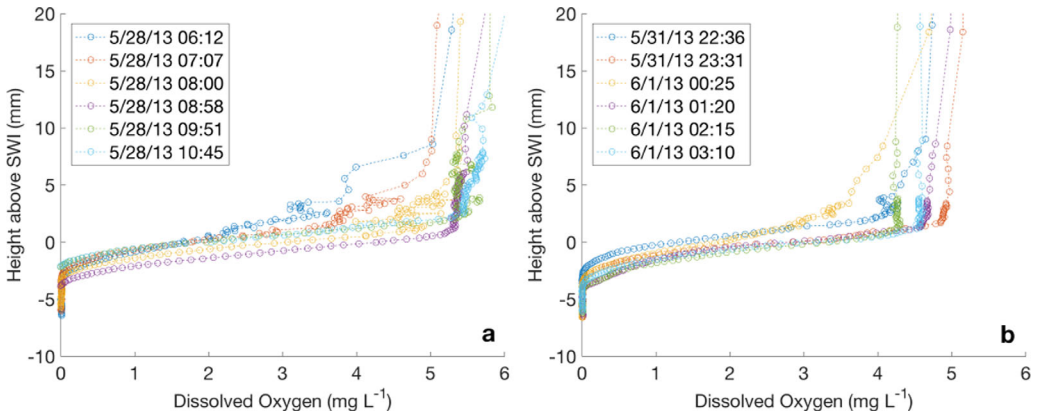

Figure 2. Example dissolved oxygen microprofiles collected during the 2013 CCR campaign on (a) May 28 (diffuser flow rate = 68 Nm^3 h^{-1}) and (b) May 31–June 1 (diffuser flow rate = 17 Nm^3 h^{-1}). See Figure 1a for sampling location.

timeframe of approximately 6 h for two different diffuser flow rates. DO concentrations measured in the bottom 10 cm of the water column with the microprofiler are displayed in Figure 3 as time series plots with the calculated J_{O2} values overlaid, along with measured δ_{DBL} and the bubble-plume diffuser gas flow rate, showing the stepped flow rate adjustment scheme.

Boxplots in Figure 4 show the impact of diffuser flow rate on J_{O2}, DO concentrations, and δ_{DBL}. DO concentrations in this portion of the water column ranged from about 3.5 to 7 mg L^{-1}. J_{O2} ranged from approximately 2–12 mmol m^{-2} d^{-1} and δ_{DBL} varied from 0.5 to 6 mm. Observed water velocities were low, less than 2.5 cm s^{-1}, with infrequent spikes up to 5 cm s^{-1}. ε calculated from this data at 15 cm above the SWI ranged from 1.6 $\times$ 10^{-12} to 1.2 $\times$ 10^{-8} W kg^{-1}, with an arithmetic mean of 5.4 $\times$ 10^{-10} W kg^{-1}. A time series of the dissipation rates is shown in supporting information Figure S1.

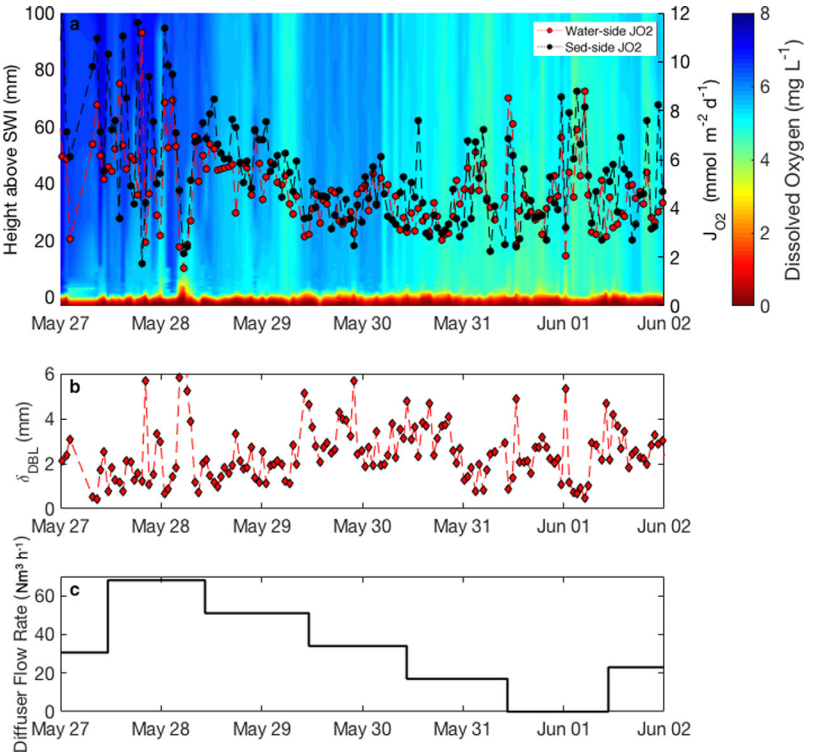

Figure 3. Time series of (a) dissolved oxygen concentration, J_{O2}, and (b) δ_{DBL}, measured with the microprofiler, and (c) the stepped oxygenation system flow rate regime during the May 2013 Carvins Cove field campaign.

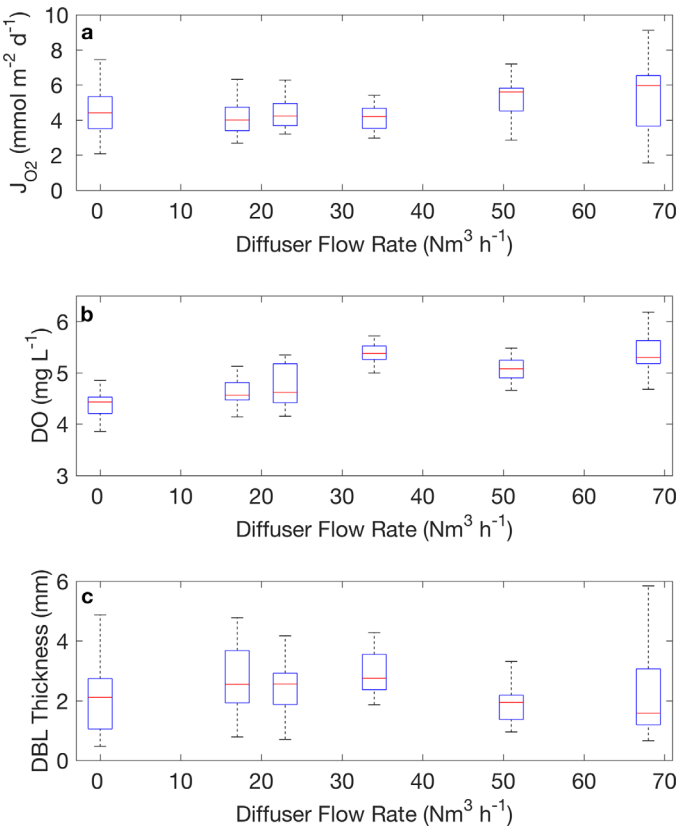

Figure 4. (a) Microprofile-derived sediment oxygen flux, (b) bulk dissolved oxygen concentrations above the sediment, and (c) diffusive boundary layer thickness plotted with oxygen diffuser flow rate (Nm^3 h^{-1}) from the May 2013 Carvins Cove field campaign. Red lines represent the mean, the blue boxes encompass the 25th–75th percentile, and the whiskers represent the maximum and minimum.

The impact of diffuser flow rates on J_{O2}, bulk water DO concentrations, and δ_{DBL} was assessed using a linear regression and the median values of these parameters (shown in Figure 4) from microprofiles collected while the diffuser was operating at various flow rates. J_{O2} showed a significant ($\alpha = 0.05$) positive correlation with diffuser flow rate (slope = 0.029; intercept = 3.81; $R^2 = 0.713$; $p = 0.0345$, n = 6). Bulk water DO concentrations also showed a significant positive correlation with diffuser flow rate (slope = 0.0138; intercept = 4.45; $R^2 = 0.68$; $p = 0.042$, n = 6). δ_{DBL} was not significantly correlated with diffuser flow rate (slope = −0.0107; intercept = 2.59; $R^2 = 0.338$; $p = 0.226$, n = 6). Visual inspection of the medians (Figure 4), however, suggest that δ_{DBL} was lower at diffuser flow rates above 50 Nm^3 h^{-1} than when the diffuser was operating at flow rates below 40 Nm^3 h^{-1}.

When the diffuser is operated at relatively high flow rates (above ~35 Nm^3 h^{-1}), the DO overlaying the SWI remains relatively high, around 6–7 mg L^{-1}, but decreases to almost 4 mg L^{-1} when the diffuser is operated at low flow rates (less than ~35 Nm^3 h^{-1}) or turned off (Figures 2 and 3). J_{O2} is, in turn, affected by these variations in DO concentration overlaying the SWI. When the diffuser is operated at relatively high flow rates, J_{O2} is also high (6–12 mmol m^{-2} d^{-1}, with an average of 5.6 mmol m^{-2} d^{-1} when the diffuser was operating at 68 Nm^3 h^{-1}). At high flow rates, δ_{DBL} is generally lower (median ~1.6 mm), but can also be quite variable, ranging from 0.7 to 5.8 mm. At lower flow rates (less than ~35 Nm^3 h^{-1}), the impact of diffuser flow rate on δ_{DBL} and J_{O2} is not as apparent. This suggests that the impact of the flow rate on δ_{DBL} and J_{O2} is minimized at low flow rates and that naturally forced hypolimnetic circulation patterns exert an equal or greater control on δ_{DBL} and J_{O2}, somewhat masking the influence of the bubble plume.

These findings indicate that, at flow rates of ~35 Nm^3 h^{-1} or lower, the primary mechanism by which CCR bubble-plume diffusers enhance J_{O2} in the near field is by increasing bulk water DO concentrations, rather than from increased mixing. Elevated DO concentrations overlaying the SWI increase the concentration gradient across the SWI, driving DO into the sediment and increasing J_{O2}. At higher flow rates (greater than ~35 Nm^3 h^{-1}), increased bulk water DO concentrations as well as increased mixing contributed to the observed increases in J_{O2}. At the two highest flow rates, bulk water DO concentrations were relatively high, and δ_{DBL} was low, resulting in higher J_{O2}.

A previous study on CCR [*Bryant et al.*, 2011a] focused on the effects of diffuser operation in the far field, finding that diffuser operation was necessary to maintain a continuous supply of DO to the SWI. When the diffuser was turned off, the water near the SWI became anoxic, and oxic conditions did not reestablish until approximately 5 days after the diffuser had been turned on. *Bryant et al.* [2011a] also observed much clearer relationships between J_{O2} and δ_{DBL} and ε than was observed in the CCR 2013 campaign. This can be partly attributed to the differences in methods for estimating ε in the two studies. The current study calculated ε

from direct measurements of velocity in the bottom boundary layer, while *Bryant et al.* [2011a] calculated ε based on δ_{DBL} as measured from oxygen microprofiles and assuming law-of-the-wall conditions. Velocity profiles in the bottom boundary layer, measured with an ADCP (Nortek Aquadopp) during the CCR 2013 field study showed that the bottom boundary layer in CCR is oscillatory and therefore often deviates from law-of-the-wall scaling. The strengthened correlation observed between J_{O2} and δ_{DBL} by *Bryant et al.* [2011a] may be due to the influence of plume detrainment in the shallower far field and/or differences in the experimental flow strategy (i.e., smaller increments in daily flow change in the current study versus extended periods of turning the oxygenation system off and on).

Gantzer et al. [2009b] also studied DO consumption in the hypolimnion of CCR as a function of diffuser flow rate. The study used DO profiles to calculate HOD and found a linear increase in HOD with increasing diffuser flow rate. *Gantzer et al.* [2009b] attributed this increase to diffuser-induced mixing (as measured by hypolimnetic warming rates), as opposed to increased hypolimnetic DO concentrations, since the data suggested that HOD was independent of DO concentrations in the hypolimnion. While J_{O2} is not directly comparable to HOD (since HOD also includes DO consumption in the water column), changes in J_{O2} would drive similar changes in HOD, as J_{O2} is often a large component of HOD. The 2013 microprofiler data show increases in J_{O2} with increasing flow rate, which would increase HOD, thus providing additional support to the *Gantzer et al.* [2009b] findings. Data from the current study also show that DO concentrations are important; however, this is in contrast to *Gantzer et al.* [2009b] conclusion. This difference in conclusions regarding the importance of hypolimnetic DO concentration may be due to the differences in measurement methods. The continuous microprofiles collected in CCR during 2013 allow the impact of hypolimnetic DO concentrations to be observed over relatively short timescales and at a single location. The HOD method of using water column DO profiles is a more coarse method, both spatially and temporally, and may not be able to capture subtle changes in HOD due to the spatial and temporal averaging inherent in calculating HOD from DO profiles.

3.2. Lake Hallwil

Interactions among the oxygenation system, DO concentrations, J_{O2}, and δ_{DBL} observed in LH were similar to those observed in CCR. Figure 5 displays the DO concentrations in the bottom 10 cm of the water column as measured with the microprofiler from 28 May to 1 June, when the microprofiler was deployed 30 m outside the diffuser ring, with calculated J_{O2} values overlaid. Example microprofiles from this deployment are also shown in Figure 6a. The six circular diffusers (Figure 1) were operating at a combined flow rate of 130 $Nm^3\ h^{-1}$ (air and oxygen mixture) before being turned off on 30 May for approximately 48 h. As observed in CCR, the DO in the water near the sediment was higher during diffuser operation (~4.5–5.5 mg L^{-1}) than when the diffusers were not in operation (~3.5–4 mg L^{-1}). J_{O2} was also significantly higher when the diffusers were operating (range: 4.5–17.5 mmol $m^{-2}\ d^{-1}$; mean = 10.7 mmol $m^{-2}\ d^{-1}$) than when the diffusers were turned off (range: 3.4–11.0 mmol $m^{-2}\ d^{-1}$; mean = 7.2 mmol $m^{-2}\ d^{-1}$), yielding an increase of nearly 50% in average J_{O2}. δ_{DBL} was slightly smaller while the diffusers were operating (range: 0.125–2.54 mm; mean = 0.61 mm) than when the diffusers were turned off (range: 0.180–2.84 mm; mean = 0.64 mm). Water velocities were typically less than 2 cm s^{-1}, but increased up to 4 cm s^{-1} for brief periods, regardless of diffuser operation (data not shown). A time series of the dissipation rates is shown in supporting information Figure S2. Dissipation rates calculated from the ADV data during this deployment ranged

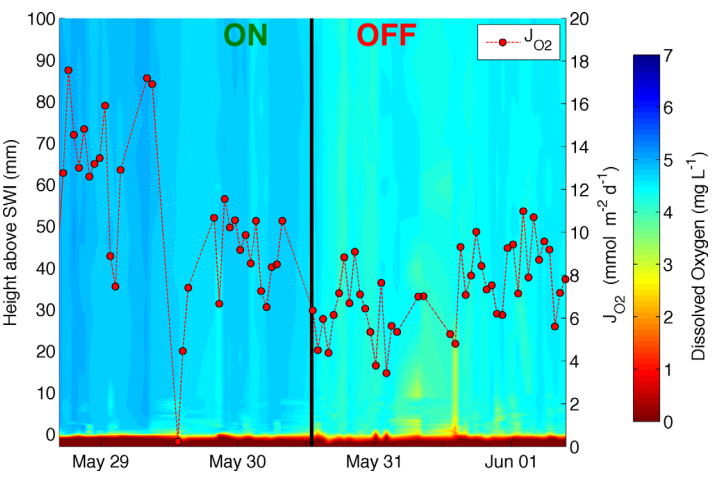

Figure 5. Time series of dissolved oxygen concentration and J_{O2} based on microprofiler data collected during the May 2012 Lake Hallwil field campaign.

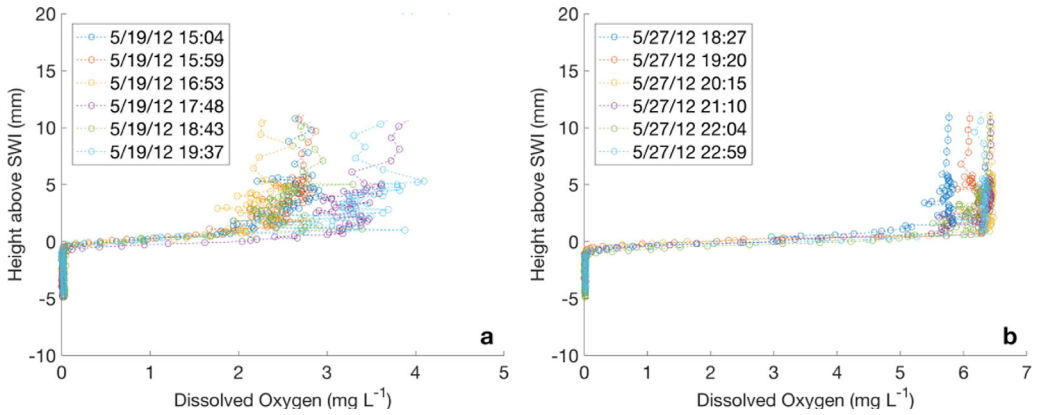

Figure 6. Example dissolved oxygen microprofiles from LH (a) during the first microprofiler deployment (~30 m from the oxygen diffuser) and (b) during the third microprofiler deployment (~3700 m from the oxygen diffuser). See Figure 1b for sampling locations.

from 4.6×10^{-12} to 1.2×10^{-8} W kg^{-1}, and there was no apparent effect of diffuser operation on the dissipation rates. Although strong seiching has been observed in Lake Hallwil previously, these motions were not particularly strong during the 2012 field campaign. As a result, impacts of periodic seiching on δ_{DBL} and J_{O2}, such as those observed in nearby Lake Alpnach by *Lorke et al.* [2003] and *Bryant et al.* [2010a] were not apparent.

Operation of the oxygen diffusers in LH seemed to enhance J_{O2} by increasing DO concentrations above the SWI with a limited effect on δ_{DBL}. When the diffusers were operating, average J_{O2} increased by 48% and DO concentrations above the SWI increased by 34%, while δ_{DBL} decreased by only 5%. Additionally, statistically significant differences are observed in J_{O2} ($p = 2.55 \times 10^{-6}$, n = 74) but not in δ_{DBL} ($p = 0.77$, n = 74) using a Student's *t* test. If δ_{DBL} is not significantly different during diffuser operation, then k_t must remain relatively constant. Thus, increased bulk water DO and the corresponding DO gradient at the SWI must be the primary drivers for the observed increases in J_{O2}.

The longitudinal transect in LH with the microprofiler showed DO microprofiles and J_{O2} to be quite spatially variable. Microprofiles near the diffuser system (Figure 6a) have a noticeably different shape than the microprofiles collected 3.7 km from the diffuser (Figure 6b). Near the diffuser system, in the deepest portion of LH, bulk water DO concentrations are relatively low, and the DO concentration above the DBL is quite variable. In contrast, the microprofiles collected 3.7 km from the diffuser show a generally constant DO concentration above the DBL, with a rapid decrease in concentrations through the DBL and into the upper 1–2 mm of the sediment. The mean and range of J_{O2} calculated from microprofiles at each of the four locations is displayed in Figure 7. J_{O2} increased with distance from the center of the diffuser ring, ranging from an average of 3.9 mmol m^{-2} d^{-1} at the site 30 m inside the diffuser ring (~26 m depth) to 12.4 mmol m^{-2} d^{-1} at the site 3700 m (~47 m depth) from the oxygen diffusers. The DO concentration near the sediment is likely a primary driver for this, given that the DO concentration also steadily increased with distance from the center of the diffuser ring (with associated decreases in water column depth). DO concentrations near the SWI were

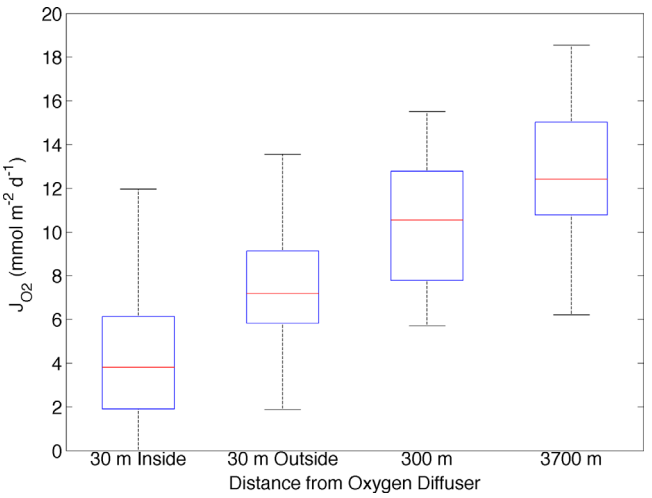

Figure 7. J_{O2} during each deployment of the microprofiler during the longitudinal transect of Lake Hallwil in 2012. The red lines represent mean J_{O2}, the blue boxes encompass the 25th–75th percentile, and the whiskers represent the maximum and minimum J_{O2}.

<3 mg L^{-1} at 30 m inside the diffuser ring ($\sim$47 m depth), $\sim$4 mg L^{-1} at 30 m outside the diffuser ring ($\sim$47 m depth), $\sim$5.5 mg L^{-1} at 300 m from the diffuser ring ($\sim$45 m depth), and $\sim$6.5 mg L^{-1} at 3700 m from the diffusers ($\sim$26 m depth). Additional factors beyond the scope of this study could also be contributing to the observed spatial pattern in J_{O2}. For example, settling organic matter and detritus may be oxidized to a variable extent in the water column before it is incorporated into the sediment. Organic matter in the deeper regions of LH may be more completely oxidized due to the increased exposure to DO (a result of both increased settling depth and oxygenation system operation) before reaching the sediment, as supported by *Müller et al*. [2012]. Organic matter in shallower portions of the lake are less affected by the oxygenation system operation and have less time to react with DO in the water column before reaching the sediment; therefore, sediments in these regions may have more labile carbon which can exert additional demand for DO, increasing J_{O2}.

Variability in J_{O2} has also been observed over much shorter spatial scales than those studied with the LH transect. Laboratory studies such as *Jørgensen and Revsbech* [1985] and *Jørgensen and Des Marais* [1990] show how J_{O2} and δ_{DBL} can vary on a mm scale. While this effect may contribute to the differences among transect sites in LH, the variability in J_{O2} across the transect sites (a factor of more than 3) is greater than that observed at finer scales (e.g., a factor of 1.5 from *Jørgensen and Des Marais* [1990]).

3.3. Field Data and Interfacial Flux Models Comparison

The low dissipation rates observed during the field campaigns suggested the possibility of long large eddy turn-over timescales; therefore, t_l was estimated using a method that does not require a long time series of very low noise data. The method is based on the analytical formulae for estimating large eddy turn-over times based on ε. By definition, $t_l = L_0/u_0$, where u_0 and L_0 are characteristic velocity scales and length scales of the energy containing eddies. *Pope* [2000] suggests taking $u_0 = k^{1/2}$. The large eddy turn-over length scale may be estimated in terms of Q and ε as $\varepsilon \sim Q^3/L_0$, therefore $L_0 \sim Q^3/\varepsilon$ [*Tennekes and Lumley*, 1972]. Q is defined as twice the turbulent kinetic energy (equation (11)). The timescales calculated using this method were often on the order of 15 min to over 60 min, which agrees with t_r estimated by back-calculating from the microprofiles.

$$Q = \left(\overline{u'^2} + \overline{v'^2} + \overline{w'^2}\right)^{1/2} = 2u_0 \tag{11}$$

Daily estimates of J_{O2} using the interfacial flux models and ADV data from CCR and LH are shown in Figures 8 and 9 along with J_{O2} calculated from microprofiles. With such low turbulent energy and long turn-over timescales, relative to the duration of a single microprofile, the microprofiles are essentially capturing instantaneous profiles rather than time-averaged profiles. Therefore, J_{O2} is displayed as a daily ensemble average. The film renewal model, u_* model, and *Lorke and Peeters* [2006] model show similar agreement with J_{O2} (waterside and sedimentside estimates based on microprofile data) in both CCR and LH, with RMSE for these three models ranging from 1.4 to 2.4 mmol m^{-2} d^{-1} in CCR and 5.2–5.9 mmol m^{-2} d^{-1} in LH (Table 2). Interestingly, all three models are based on different characteristics of turbulent flow. The film renewal model and Lorke and Peeters models are based on very different scales and yet yield similar results. The large eddy turnover length scale for the large eddy-based model in the CCR and LH studies is on the order of 10 m, while the Batchelor length scale is on the order of 10^{-3} to 10^{-4} m. The u_* model is based on shear stress at the SWI and yet also yields similar estimates of J_{O2}. The RMSE shown in Table 2 suggest that the film renewal model (RMSE = 5.2 mmol m^{-2} d^{-1}) may provide a slightly improved fit over the Lorke and Peeters model (RMSE = 5.9 mmol m^{-2} d^{-1}) and u_* model (RMSE = 5.7 mmol m^{-2} d^{-1}) in LH, while the u_* model (RMSE = 1.4 mmol m^{-2} d^{-1}) provides the best fit in CCR, performing slightly better than the film renewal model (RMSE = 1.6 mmol m^{-2} d^{-1}) and the Lorke and Peeters model (RMSE = 2.4 mmol m^{-2} d^{-1}). The RMSE values for CCR range from 20 to 59% of the J_{O2} calculated from the microprofiles. RMSE as a fraction of the microprofile-based J_{O2} in LH is much larger, ranging from 24 to 210% when the data from all four deployments are considered collectively. While these RMSE values can be relatively high at times compared to the magnitude of the J_{O2} measurements, they are similar in magnitude to reported RMSE for other models of J_{O2}. For example, RMSE reported by *Brady et al*. [2013] for a model of J_{O2} was also on the order of 20 to $>$100% of the observed J_{O2}. The differences among the RMSE from the models applied to CCR and LH are relatively small and may be a result of the relatively limited sample size (n = 6 for CCR; n = 11 for LH).

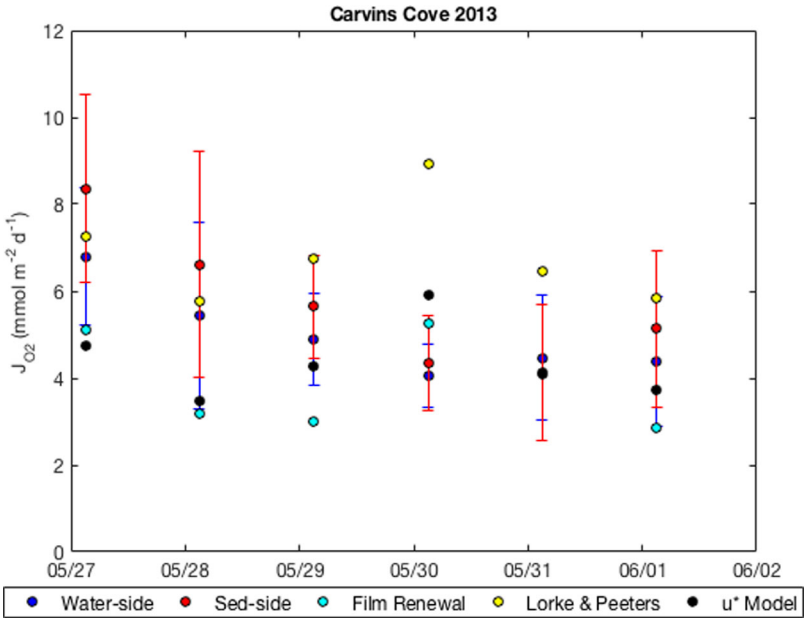

Figure 8. J_{O2} calculated from the microprofiles compared to J_{O2} calculated from interfacial flux models for the 2013 Carvins Cove field campaign. The error bars encompass the range of microprofile-based J_{O2} values for each daily average.

Similar studies comparing J_{O2} to interfacial flux models based entirely on in situ measurements are somewhat limited in the literature. *Nakamura and Stefan* [1994] compared a model of interfacial flux (as a function of flow velocity) to data collected from in situ flux chambers by *Boynton et al.* [1981], which accurately reproduced the measured J_{O2}. While flux chambers have the advantage of collecting J_{O2} measurements in situ from relatively undisturbed sediments, they also isolate the overlaying water column from the surrounding hydrodynamics. The mixing induced in the flux chamber (via pumps or otherwise) may not be representative of the natural hydrodynamic forcing. *Mackenthun and Stefan* [1998] provided further support for the *Nakamura and Stefan* [1994] model with laboratory flume measurements using three different

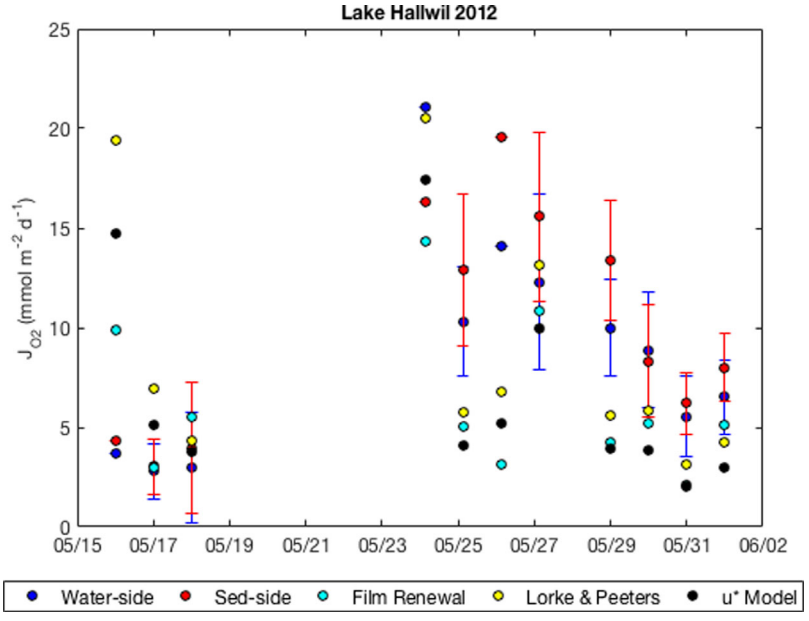

Figure 9. J_{O2} calculated from the microprofiles compared to J_{O2} calculated from interfacial flux models for the Lake Hallwil field campaign (May 2012). The error bars encompass the range of microprofile-based J_{O2} values for each daily average.

Table 2. Root Mean Squared Error (RMSE) From Comparing 24 h Averages of J_{O2} to Calculated J_{O2} From Interfacial Flux Models (n = Number of Data Points)[a]

	Film Renewal	u* Model	Lorke and Peeters	n
CCR 2013	1.6	1.4	2.4	6
LH1	3.9	6.6	9.4	3
LH2	6.1	5.1	3.3	2
LH3	7.8	6.5	5.2	2
LH4	3.9	4.7	3.1	4
LH (all)	5.2	5.7	5.9	11

[a]RMSE is given in mmol m^{-2} d^{-1}.

sediment types. Laboratory measurements, however, often result in sediment disturbances during collection and transport may fail to reproduce larger-scale hydrodynamics that may influence J_{O2}.

O'Connor et al. [2009] compared experimental measurements of J_{O2} from a recirculating flume [*O'Connor and Hondzo*, 2008a, 2008b] to the Lewis-Whitman, film-renewal, and u_* models, finding the film-renewal model to provide the best estimates of k_t. For their study, *O'Connor and Hondzo* [2008a] used particle image velocimetry (PIV) to characterize the renewal frequency used for the film-renewal model, basing r on the period between sweep and eject motions measured with their PIV and ADV experimental setup. The comparisons made in the current study using in situ data collected in CCR and LH also provide support for the film-renewal model.

In their paper, *Lorke and Peeters* [2006] call for a "new generation of experiments" which couple turbulence measurements with estimates of k_t, as done in the current study, to test the proposed universal scaling relationship given in equation (9). To our knowledge, the current study is the first to compare various models of k_t to simultaneous in situ field measurements of J_{O2}, velocity, and turbulence. Figure 10 presents the transfer velocities calculated using J_{O2} measurements, normalized by the Schmidt number, as a function of the observed ε. The line representing the Lorke and Peeters model agrees quite well with the observed transfer velocities in CCR, but shows somewhat less agreement with the observed k_t in LH, especially at low ε values. While the in situ data collected in CCR and LH supports the idea that this model could represent a universal model for calculating k_t, the J_{O2} calculated using this model does not appear to be a marked improvement over J_{O2} as calculated by the film renewal or u_* models (Figures 8 and 9).

4. Conclusions

Hypolimnetic oxygenation is a lake management strategy that is becoming increasingly common, particularly the use of bubble-plume oxygenation systems. Despite their capability to increase hypolimnetic DO concentrations in deep lakes and reservoirs, oxygenation systems typically stimulate an increase in DO consumption, the magnitude of which is difficult to predict accurately during system design. Field studies in CCR and LH both showed the capability of bubble-plume oxygenation systems to influence near-sediment DO concentrations and J_{O2}. When the oxygenation systems are operating and supplying additional DO to the hypolimnion, the DO concentration in the bulk hypolimnetic water increases and creates a stronger

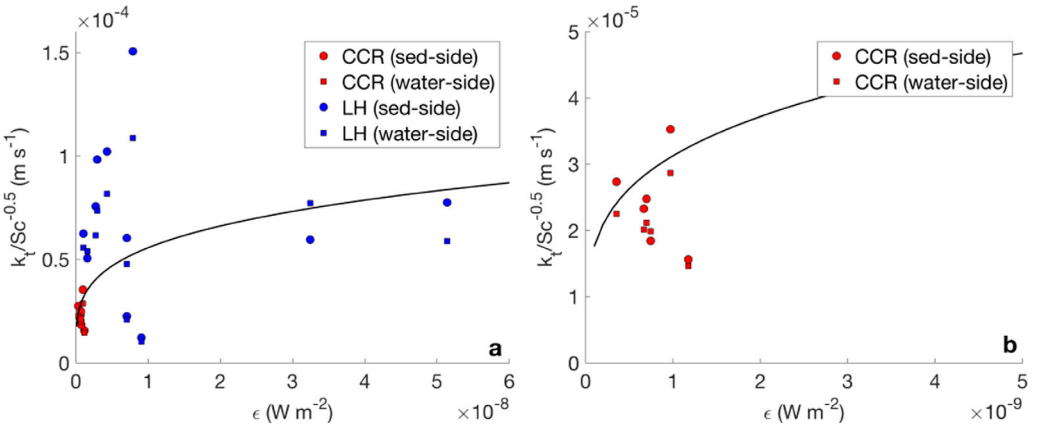

Figure 10. Observed transfer velocity (k_t), calculated from oxygen microprofiles collected during the 2012 Lake Hallwil (LH) and 2013 Carvins Cove Reservoir (CCR) field campaigns, normalized by the Schmidt number (Sc) and plotted versus the observed turbulence dissipation rate (ε). The black line represents the universal scaling relationship proposed by *Lorke and Peeters* [2006]. Data in Figure 10b are identical to the data in Figure 10a, but at a different scale to better compare the data from CCR to the relationship from *Lorke and Peeters* [2006].

concentration gradient across the SWI. This drives additional DO to the SWI which leads to enhanced J_{O2}, as observed in both field studies. If these oxygenation-induced increases in sediment oxygen uptake are not taken into account, oxygenation strategies are at risk of failing to properly combat hypolimnetic oxygen depletion and improve source-water quality. In both field studies, J_{O2} was on the order of 1.5–2 times higher during diffuser operation, relative to J_{O2} when the diffusers were turned off, which provides some support for the use of safety factors in the range of 2–4 for oxygenation system design.

DO dynamics near the SWI were shown to be quite variable across several scales. Microprofiles collected during each deployment show the unsteady behavior of DO and J_{O2} under varying gas-addition rates at a single location. Additionally, J_{O2} was observed to be quite variable within LH, as well as variable between the two oxygenated lakes. The timescales of turbulent mixing in the BBL estimated from the ADV data were also observed to be quite long in these two low-energy systems.

The model evaluation performed during this study highlights tools that may be valuable to water managers and utilities for estimating oxygenation-induced DO uptake and resultant oxygenation needs. The film renewal model, u_* model, and Lorke and Peeters models scale with values of J_{O2} calculated from DO microprofiles, with RMSE less than 6 mmol m^{-2} d^{-1} in LH and less than 2.5 mmol m^{-2} d^{-1} in CCR, despite being based on very different characteristics of turbulent flows. The data also support and give greater confidence to the universal scaling relationship for interfacial flux proposed by *Lorke and Peeters* [2006]. The interfacial flux models could be appropriate to include in hydrodynamic models to link lake hydrodynamics to J_{O2}. Incorporating these interfacial flux models into a hydrodynamic model could lead to improvements in design and operation of hypolimnetic oxygenation systems by refining our ability to predict the spatial and temporal variability in J_{O2} in response to oxygenation system operations.

Acknowledgments
The data associated with this manuscript are available from the authors. The research was funded by a U.S. National Science Foundation grant CBET 1033514. We would like to thank the Western Virginia Water Authority for access to Carvins Cove Reservoir and Kanton Aargau for access to Lake Hallwil during the field campaigns. We also thank Michi Schurter of Eawag, Arno Stöckli of Kanton Aargau, and Christina Urbanczyk for their valuable assistance during the field campaigns.

References

American Water Works Association (2010), *Water Quality and Treatment: A Handbook on Drinking Water*, edited by J. Edzwald, 6th ed., McGraw Hill, New York.
Batchelor, G. K. (1959), Small-scale variation of convected quantities like temperature in turbulent fluid, *J. Fluid Mech.*, *5*(1), 113–133.
Beutel, M. W. (2003), Hypolimnetic anoxia and sediment oxygen demand in California drinking water reservoirs, *Lake Reservoir Manage.*, *19*(3), 208–221.
Beutel, M. W. (2006), Inhibition of ammonia release from anoxic profundal sediments in lakes using hypolimnetic oxygenation, *Ecol. Eng.*, *28*(3), 271–279.
Beutel, M. W., and A. J. Horne (1999), A review of the effects of hypolimnetic oxygenation on lake and reservoir water quality, *Lake Reservoir Manage.*, *15*(4), 285–297.
Beutel, M. W., T. M. Leaonard, S. R. Dent, and B. C. Moore (2008), Effects of aerobic and anaerobic conditions on P, N, Fe, Mn, and Hg accumulation in waters overlaying profundal sediments of an oligo-mesotrophic lake, *Water Res.*, *42*(8–9), 1953–1962.
Boynton, W. R., W. M. Kemp, C. G. Osborne, K. R. Kaumeyer, and M. C. Jenkins (1981), Influence of water circulation rate on in situ measurements of benthic community respiration, *Mar. Biol.*, *65*, 185–190.
Brady, D. C., J. M. Testa, D. M. Di Toro, W. R. Boynton, and W. M. Kemp (2013), Sediment flux modeling: Calibration and application for coastal systems, *Estuarine Coastal Shelf Sci.*, *117*, 107–124.
Bryant, L. D., C. Lorrai, D. F. McGinnis, A. Brand, A. Wüest, and J. C. Little (2010a), Variable sediment oxygen uptake in response to dynamic forcing, *Limnol. Oceanogr.*, *55*(2), 950–964.
Bryant, L. D., D. F. McGinnis, C. Lorrai, A. Brand, J. C. Little, and A. Wüest (2010b), Evaluating oxygen fluxes using microprofiles from both sides of the sediment-water interface, *Limnol. Oceanogr. Methods*, *8*, 610–627.
Bryant, L. D., P. A. Gantzer, and J. C. Little (2011a), Increased sediment oxygen uptake caused by oxygenation-induced hypolimnetic mixing, *Water Res.*, *45*(12), 3692–3703.
Bryant, L. D., H. Hsu-Kim, P. A. Gantzer, and J. C. Little (2011b), Solving the problem at the source: Controlling Mn release at the sediment-water interface via hypolimnetic oxygenation, *Water Res.*, *45*(19), 6381–6392.
Dalsgaard, T., et al. (2000), *Protocol Handbook for NICE—Nitrogen Cycling in Estuaries: A Project Under the EU Research Programme: Marine Science and Technology (MAST III)*, Natl. Environ. Res. Inst., Silkeborg, Denmark.
Danckwerts, P. V. (1951), Significance of liquid-film coefficients in gas absorption, *Ind. Eng. Chem.*, *43*(6), 1460–1467.
Davison, W. (1993), Iron and manganese in lakes, *Earth Sci. Rev.*, *34*, 119–163.
Debroux, J. F., M. W. Beutel, C. M. Thompson, and S. Mulligan (2012), Design and testing of a novel hypolimnetic oxygenation system to improve water quality in Lake Bard, California, *Lake Reservoir Manage.*, *28*(3), 245–254.
Funkey, C. P., D. J. Conley, N. S. Reuss, C. Humborg, T. Jilbert, and C. P. Slomp (2014), Hypoxia sustains cyanobacteria blooms in the Baltic Sea, *Environ. Sci. Technol.*, *48*(5), 2598–2602.
Gantzer, P. A., L. D. Bryant, and J. C. Little (2009a), Controlling soluble iron and manganese in a water-supply reservoir using hypolimnetic oxygenation, *Water Res.*, *43*(5), 1285–1294.
Gantzer, P. A., L. D. Bryant, and J. C. Little (2009b), Effect of hypolimnetic oxygenation on oxygen depletion rates in two water-supply reservoirs, *Water Res.*, *43*(6), 1700–1710.
Grant, H. L., R. W. Stewart, and A. Moillet (1962), Turbulence spectra from a tidal channel, *J. Fluid Mech.*, *12*(2), 241–268.
Higashino, M., C. Gantzer, and H. Stefan (2004), Unsteady diffusional mass transfer at the sediment/water interface: Theory and significance for SOD measurement, *Water Res.*, *38*(1), 1–12.

Higbie, R. (1935), The rate of absorption of a pure gas into a still liquid during short periods of exposure, *Trans. Am. Inst. Chem. Eng.*, *31*, 365–389.
Holzner, C. P., Y. Tomonaga, A. Stöckli, N. Denecke, and R. Kipfer (2012), Using noble gases to analyze the efficiency of artificial aeration in Lake Hallwil, Switzerland, *Water Resour. Res.*, *48*, W09531, doi:10.1029/2012WR012030.
Jørgensen, B. B., and D. J. Des Marais (1990), The diffusive boundary layer of sediments: Oxygen microgradients over a microbial mat, *Limnol. Oceanogr.*, *35*(6), 1343–1355.
Jørgensen B. B., and N. P. Revsbech (1985), Diffusive boundary layers and the oxygen uptake of sediments and detritus, *Limnol. Oceanogr.*, *30*(1), 111–122.
Kohl, P., and S. Medlar (2003), *Occurrence of Manganese in Drinking Water and Manganese Control*, AWWA Res. Found., Denver, Colo.
King, C. J. (1966), Turbulent liquid phase mass transfer at a free gas-liquid interface, *Ind. Eng. Chem. Fundam.*, *5*(1), 1–8.
Lewis, W. K., and W. G. Whitman (1924), Principles of gas absorption, *Ind. Eng. Chem.*, *16*(12), 1215–1220.
Liboriussen, L., M. Søndergaard, E. Jeppesen, I. Thorsgaard, S. Grünfeld, T. S. Jakobsen, and K. Hansen (2009), Effects of hypolimnetic oxygenation on water quality: Results from five Danish lakes, *Hydrobiologia*, *625*(1), 157–172.
Lorke, A., and F. Peeters (2006), Toward a unified scaling relation for interfacial fluxes, *J. Phys. Oceanogr.*, *36*(5), 955–961.
Lorke, A., L. Umlauf, T. Jonas, and A. Wüest, (2002), Dynamics of turbulence in low-speed oscillating bottom-boundary layers of stratified basins, *Environ. Fluid Mech.*, *2*(4), 291–313.
Lorke, A., B. Müller, M. Maerki, and A. Wüest (2003), Breathing sediments: The control of diffusive transport across the sediment-water interface by periodic boundary-layer turbulence, *Limnol. Oceanogr.*, *48*(6), 2077–2085.
Mackenthun, A. A., and H. G. Stefan (1998), Effect of Flow Velocity on Sediment Oxygen Demand: Experiments, *J. Environ. Eng.*, *124*(3), 222–230.
McGinnis, D. F., A. Lorke, A. Wüest, A. Stöckli, and J. C. Little (2004), Interaction between a bubble plume and the near field in a stratified lake, *Water Resour. Res.*, *40*(10), W10206, doi:10.1029/2004WR003038.
Müller, B., L. D. Bryant, A. Matzinger, and A. Wüest (2012), Hypolimnetic oxygen depletion in eutrophic lakes, *Environ. Sci. Technol.*, *46*(18), 9964–9971.
Müller, B., R. Gächter, and A. Wüest (2014), Accelerated water quality improvement during oligotrophication in peri-alpine lakes, *Environ. Sci. Technol.*, *48*(12), 6671–6677.
Moore, B. C., P. Chen, W. H. Funk, and D. Yonge (1996), A model for predicting lake sediment oxygen demand following hypolimnetic aeration, *Water Resour. Bull.*, *32*(4), 723–731.
Nakamura, Y., and H. G. Stefan (1994), Effect of flow velocity on sediment oxygen demand: Theory, *J. Environ. Eng.*, *120*(5), 996–1016.
O'Connor, B. L., and M. Hondzo (2008a), Dissolved oxygen transfer to sediments by sweep and eject motions in aquatic environments, *Limnol. Oceanogr.*, *53*(2), 566–578.
O'Connor, B. L., and M. Hondzo (2008b), Enhancement and inhibition of denitrification by fluid-flow and dissolved oxygen flux to stream sediments, *Environ. Sci. Technol.*, *42*(1), 119–125.
O'Connor, B. L., M. Hondzo, and J. W. Harvey (2009), Incorporating both physical and kinetic limitations in quantifying dissolved oxygen flux to aquatic sediments, *J. Environ. Eng.*, *135*(12), 1304–1314.
Pope, S. B. (2000), *Turbulent Flows*, Cambridge Univ. Press, Cambridge, U. K.
Schwefel, R., A. Gaudard, A. Wüest, and D. Bouffard (2016), Effects of climate change on deepwater oxygen and winter mixing in a deep lake (Lake Geneva): Comparing observational findings and modeling, *Water Resour. Res.*, *52*(11), 8811–8826, doi:10.1002/2016WR019194.
Singleton, V. L., and J. C. Little (2006), Designing hypolimnetic aeration and oxygenation systems—A review, *Environ. Sci. Technol.*, *40*(24), 7512–7520.
Singleton, V. L., F. J. Rueda, and J. C. Little (2010), A coupled bubble plume-reservoir model for hypolimnetic oxygenation, *Water Resour. Res.*, *46*, W12538, doi:10.1029/2009WR009012.
Tennekes, H., and J. L. Lumley (1972), *A First Course in Turbulence*, MIT Press, Cambridge, Mass.
Testa, J. M., and W. M. Kemp (2012), Hypoxia-induced shifts in nitrogen and phosphorus cycling in Chesapeake Bay, *Limnol. Oceanogr.*, *57*(3), 835–850.
Toor, H. L., and J. M. Marchello (1958), Film-penetration model for mass and heat transfer, *AIChE J.*, *4*(1), 97–101.